



Instrument
inter-comparison of
glyoxal, methyl
glyoxal and NO₂

R. Thalman et al.

This discussion paper is/has been under review for the journal Atmospheric Measurement Techniques (AMT). Please refer to the corresponding final paper in AMT if available.

Instrument inter-comparison of glyoxal, methyl glyoxal and NO₂ under simulated atmospheric conditions

R. Thalman^{1,2,*}, M. T. Baeza-Romero³, S. M. Ball⁴, E. Borrás⁵, M. J. S. Daniels⁴, I. C. A. Goodall⁴, S. B. Henry⁶, T. Karl^{7,8}, F. N. Keutsch⁶, S. Kim^{7,9}, J. Mak¹⁰, P. S. Monks⁴, A. Muñoz⁵, J. Orlando⁷, S. Peppe¹¹, A. R. Rickard^{12,**}, M. Ródenas⁵, P. Sánchez⁵, R. Seco^{7,9}, L. Su¹⁰, G. Tyndall⁷, M. Vázquez⁵, T. Vera⁵, E. Waxman^{1,2}, and R. Volkamer^{1,2}

¹Department of Chemistry and Biochemistry, University of Colorado Boulder, Boulder, CO, USA

²Cooperative Institute for Research in Environmental Sciences (CIRES), Boulder, CO, USA

³Escuela de Ingeniería Industrial de Toledo, Universidad de Castilla la Mancha, Toledo, Spain

⁴Department of Chemistry, University of Leicester, Leicester, LE1 7RH, UK

⁵Instituto Universitario UMH-CEAM, Valencia, Spain

⁶University Wisconsin, Madison, USA

⁷National Center for Atmospheric Research, Boulder, CO, USA

⁸University of Innsbruck, Innsbruck, Austria

⁹University of California, Irvine, CA, USA

Title Page

Abstract

Introduction

Conclusions

References

Tables

Figures



Back

Close

Full Screen / Esc

Printer-friendly Version

Interactive Discussion



**Instrument
inter-comparison of
glyoxal, methyl
glyoxal and NO₂**

R. Thalman et al.

Title Page

Abstract

Introduction

Conclusions

References

Tables

Figures



Back

Close

Full Screen / Esc

Printer-friendly Version

Interactive Discussion

¹⁰State University of New York, Stony Brook, New York, USA¹¹School of Earth and Environment, University of Leeds, Leeds, UK¹²National Centre for Atmospheric Science, School of Chemistry, University of Leeds, Leeds, UK^{*}now at: Brookhaven National Laboratory, Upton, NY, USA^{**}now at: National Centre for Atmospheric Science, Wolfson Atmospheric Chemistry Laboratories, Department of Chemistry, University of York, York, UK

Received: 2 July 2014 – Accepted: 5 August 2014 – Published: 19 August 2014

Correspondence to: R. Volkamer (rainer.volkamer@colorado.edu)

Published by Copernicus Publications on behalf of the European Geosciences Union.

2 Instrumentation and experimental conditions

2.1 Instruments

5 The various instruments used at both the NCAR and EUPHORE facility are listed in Table 1, and described in the following subsections in more detail.

2.1.1 NCAR Fourier transform infrared spectrometer (FTIR)

The FTIR instrument is integrated as part of the NCAR chamber, and measures along the long-axis of the chamber (2 m long, 16 passes, giving a total light path of 32 m).
10 The spectrometer consists of a BOMEM DA3.01 FTIR, and was operated at 1 cm^{-1} resolution and collected and averaged 200 spectra between 800 and 4000 cm^{-1} over a period of 4 min. Standard spectra used for spectral subtraction were obtained using the same conditions as above, from scans of samples prepared via injection of known quantities of analyte into the chamber. Absorption cross sections quoted are derived
15 from these standard spectra.

2.1.2 NCAR proton transfer reaction time of flight mass spectrometer (PTR-ToF-MS)

The NCAR chamber experiment involved measurements of VOCs by using a high resolution PTR-ToF-MS (Ionicon Analytik GmbH, Innsbruck, Austria) (Jordan et al., 2009).
20 For detailed review of the instrumentation, refer to de Gouw and Warneke (2007). During the experiment, the PTR-ToF-MS was operated under H_3O^+ mode, which uses hydronium ions (H_3O^+) as the primary reagent ions to protonate VOC species. The ionization conditions in the drift tube were controlled by setting the drift voltage at 542 V,

Instrument inter-comparison of glyoxal, methyl glyoxal and NO_2

R. Thalman et al.

Title Page

Abstract

Introduction

Conclusions

References

Tables

Figures



Back

Close

Full Screen / Esc

Printer-friendly Version

Interactive Discussion



Instrument inter-comparison of glyoxal, methyl glyoxal and NO₂

R. Thalman et al.

Title Page

Abstract

Introduction

Conclusions

References

Tables

Figures

◀

▶

◀

▶

Back

Close

Full Screen / Esc

Printer-friendly Version

Interactive Discussion



Analysis of CE-DOAS spectra was performed for the retrieval of glyoxal, methyl glyoxal, NO₂ and O₄ as described in Thalman and Volkamer (2010). The mirror reflectivity was calibrated from the differential Rayleigh scattering of helium and nitrogen (Washenfelder et al., 2008) using the Rayleigh scattering cross-section values as described in Thalman et al. (2014). The mirror reflectivity curve was then used to calculate the absorption path in the empty cavity:

$$L(\lambda) = \frac{d_s}{1 - R(\lambda) + \alpha_{\text{Ray}}^{\text{Air}} d_0 + \sigma_{\text{O}_4} N_d^2 \text{O}_2^2{}_{2,\text{mixingratio}} d_s + \sigma_i c_i d_s} = \frac{\text{O}_{4\text{SCD}}}{N_d^2 \text{O}_2^2{}_{2,\text{mixingratio}}} \quad (1)$$

Where $L(\lambda)$ is the effective path length with respect to wavelength (cm), d_s is the sample length (cm), $R(\lambda)$ is the mirror reflectivity with respect to wavelength, α is the extinction due to the Rayleigh scattering in air (cm⁻¹), d_0 is the cavity length (cm), σ_i is the absorption cross-section of the corresponding gas, N_d is the density (molecules cm⁻³), c_i is the concentration of the corresponding gas (molecules cm⁻³), and $\text{O}_{4\text{SCD}}$ is the slant column density (concentration × pathlength of O₄, cm⁻⁵ molecule²). Absorption cross-sections are scaled by the path length (usually a maximum of 15 km for the sample path) as outlined in Thalman and Volkamer (2010). The Windoas software (Fayt and Van Roosendael, 2001) was used to adjust literature cross sections to the instrument resolution, and perform DOAS fitting of multiple reference spectra simultaneously. Literature absorption cross-sections for glyoxal (Volkamer et al., 2005b), methyl glyoxal (Meller et al., 1991), NO₂ (Vandaele et al., 2002), and O₄ (Hermans et al., 1999; Hermans, 2010) were used in fitting the spectra. The DOAS output in units of slant column density (SCD = concentration · L) was then divided by the path length to get concentration. Measurements of O₄ SCDs as part of each spectrum at high signal-to-noise facilitate online control over cavity alignment and/or R . The path length calculated from Eq. (1) agreed with the O₄ calibration gas within 1%. Equation (1) was solved iteratively to account for self-limitation until the concentrations converge (either for NO₂ (experiments 3, 4, 7, 9 and 10) or glyoxal (exp 1 and 8)). For experiments with

Instrument inter-comparison of glyoxal, methyl glyoxal and NO₂

R. Thalman et al.

Title Page

Abstract

Introduction

Conclusions

References

Tables

Figures

◀

▶

◀

▶

Back

Close

Full Screen / Esc

Printer-friendly Version

Interactive Discussion



during standard field operation. The variability of the alignment is reflected in variability of the calibration factors. The detection axis is orthogonal to both the laser and gas axis. The detector is a single photon counting photo-multiplier tube (PMT) guarded by a 520 ± 20 nm bandpass filter (Barr Associates). The interior of the detection cell was optically baffled to reduce laser and ambient light scattering and/or reflecting into the detector.

The Mad-LIP instrument detects both glyoxal and methyl glyoxal by phosphorescence. This is initiated in either analyte by absorption of the laser light, after which, they relax by emission of a phosphorescent photon or are quenched collisionally. As a result, the amount of phosphorescent photons emitted by either is linearly proportional to the optical cross section, which is a function of wavelength described by their respective absorption spectra, the intensity of light, and analyte number density. Both glyoxal and methyl glyoxal signals are normalized by laser power to account for its variation. The photons between 2.5 and 37.5 μ s after each laser pulse during a period of integration are summed and recorded as the signal during this time. Due to this gate and delay photon counting combined with a 520 ± 5 nm bandpass filter, the effect from laser scatter and fluorescent photons are diminished, minimizing the signal background, and, in particular eliminating any detection of NO₂ fluorescence.

The PMT signal (S_{total}) is a linear combination of several components: dark counts (S_{dark}), light scatter (S_{scatter}), glyoxal phosphorescence (S_{gly}) and methyl glyoxal phosphorescence (S_{mgly}). The glyoxal mixing ratio ($\text{Glyoxal}_{\text{mr}}$) is proportional to the difference in S_{total} at two different wavelengths: one at high glyoxal absorbance ($\lambda_1 = 440.138$ nm) and another at low glyoxal absorbance ($\lambda_2 = 440.104$ nm, Fig. S4 in the Supplement, Eq. 3). S_{total} is expressed in Eq. (2), followed by the calculation of $\text{Glyoxal}_{\text{mr}}$ in Eq. (3).

$$S(\lambda)_{\text{total}} = S_{\text{dark}} + S_{\text{scatter}} + S(\lambda)_{\text{gly}} + S_{\text{mgly}} \quad (2)$$

$$\begin{aligned} \text{Glyoxal}_{\text{mr}} &= [S(\lambda_1)_{\text{total}} - S(\lambda_2)_{\text{total}}] \cdot \eta_{\text{gly}} \\ &= [[S_{\text{dark}} + S_{\text{scatter}} + S(\lambda_1)_{\text{gly}} + S_{\text{mgly}}] - [S_{\text{dark}} + S_{\text{scatter}} + S(\lambda_2)_{\text{gly}} + S_{\text{mgly}}]] \end{aligned}$$

$$\begin{aligned}
 &= \cdot \eta_{\text{gly}} \\
 &= [S(\lambda_1)_{\text{gly}} - S(\lambda_2)_{\text{gly}}] \cdot \eta_{\text{gly}} \quad (3)
 \end{aligned}$$

Where η_{gly} is the calibration factor relating glyoxal mixing ratio to the net glyoxal signal ($S(\lambda_1)_{\text{gly}} - S(\lambda_2)_{\text{gly}}$). The intensity of dark counts is a characteristic of the PMT, and light scatter as well as methyl glyoxal absorption are the same at λ_1 and λ_2 . The calibration factor is determined by introducing a known amount of glyoxal by diluting a calibration standard quantified by CRDS and introducing it into the White-type multi-pass cell. See the following sub-section for CRDS system description as well as theory of operation.

A very high degree of selectivity for glyoxal is achieved using this wavelength dithering approach coupled with monitoring only phosphorescent emission. Only molecules that absorb at ~ 440 nm, phosphoresce at ~ 520 nm, and have similar absorption spectra to glyoxal would be able to interfere. To the authors' knowledge, the Mad-LIP instrument has not observed any interferences with glyoxal detection.

Because S_{gly} is proportional to the glyoxal optical cross section at λ_1 ($1.02 \times 10^{-18} \text{ cm}^2 \text{ molecule}^{-1}$), and the net glyoxal signal is proportional to the difference in optical cross section at λ_1 and λ_2 ($3.42 \times 10^{-19} \text{ cm}^2 \text{ molecule}^{-1}$, Volkamer et al., 2005b), the contribution of glyoxal at λ_1 is calculated in Eq. (4). This is then substituted into Eq. (2), and is solved for S_{mgly} , and related to the mixing ratio of methyl glyoxal (methyl glyoxal_{mr}) by a calibration factor (η_{mgly}).

$$S(\lambda_1)_{\text{gly}} = \left(\frac{\sigma(\lambda_1)_{\text{gly}}}{\sigma(\lambda_1)_{\text{gly}} - \sigma(\lambda_2)_{\text{gly}}} \right) \cdot (S(\lambda_1)_{\text{gly}} - S(\lambda_2)_{\text{gly}}) \quad (4)$$

$$\begin{aligned}
 \text{Methylglyoxal}_{\text{mr}} = & \left[S(\lambda)_{\text{total}} - S_{\text{dark}} - S_{\text{scatter}} - \left(\frac{\sigma(\lambda_1)_{\text{gly}}}{\sigma(\lambda_1)_{\text{gly}} - \sigma(\lambda_2)_{\text{gly}}} \right) \right. \\
 & \left. \cdot (S(\lambda_1)_{\text{gly}} - S(\lambda_2)_{\text{gly}}) \right] \cdot \eta_{\text{mgly}} \quad (5)
 \end{aligned}$$

Instrument inter-comparison of glyoxal, methyl glyoxal and NO₂

R. Thalman et al.

Title Page

Abstract

Introduction

Conclusions

References

Tables

Figures

◀

▶

◀

▶

Back

Close

Full Screen / Esc

Printer-friendly Version

Interactive Discussion



including a curve that models and subtracts it locally. The software as been tested and used in previous works (Muñoz et al., 2011, 2012).

Reference spectra were previously collected with the instrument, and calibrated with the references used by the W-DOAS system (Sect. 2.1.3). Water, formaldehyde, methanol and other compounds show absorption bands in the same spectral region as glyoxal and methyl glyoxal. Together with these compounds, the instrument was used to report the evolution of most of the reactants and products forming the complex mixture in the experiments preformed. These compounds were present in the samples to a greater or lesser degree depending on the experiment carried out. The fitting was done using both the aldehydic C-H band and the region 770–1140 cm⁻¹. The list of compounds analyzed includes ozone, isoprene, nitric acid, *o*-xylene, and formic acid. SF₆ was also monitored by FTIR to quantify the dilution range of the chamber.

2.1.9 CEAM Solid-phase-microextraction (SPME)

Solid Phase Microextraction (SPME) methodology was used to determine glyoxal and methyl glyoxal through PFBHA on-fiber derivatization. A detailed description of the methodology used at the EUPHORE chambers can be found in the literature (Gómez Alvarez et al., 2007; Alvarez and Valcárcel, 2009). Briefly, the SPME device used in this work consisted of a holder assembly with 65 μm fibers coated with Polydimethylsiloxane/Divinylbenzene (PDMS/DVB), from Supelco, Bellefonte, PA (USA). These fibers were conditioned following the manufacturer's recommendations for at least 0.5 h at 250 °C to eliminate any impurities. Fibers were loaded with PFBHA derivatization reagent, for 2 min, through the headspace of a 4 mL opaque amber vial containing a 17 mg mL⁻¹ PFBHA water solution.

Exposing the fiber to the air of the chamber was achieved by means of an aluminum adapter located in one of the flanges in the chamber floor. In the exposed position, fibers extend into the chamber by a few millimeters.

Samples were taken for several minutes and were subsequently analyzed by GC-FID by injecting the fiber directly into the GC injector. Sampling time ranged depending on

Instrument inter-comparison of glyoxal, methyl glyoxal and NO₂

R. Thalman et al.

Title Page

Abstract

Introduction

Conclusions

References

Tables

Figures



Back

Close

Full Screen / Esc

Printer-friendly Version

Interactive Discussion



hydroxyacetone (isoprene). In addition a reasonable amount of SOA is formed in the *o*-xylene experiment.

Glyoxal and methyl glyoxal were prepared as described in the literature: pure glyoxal monomer was prepared from the solid trimer-dihydrate using the methods described in (Feierabend et al., 2007) with minor modification. Pure methyl glyoxal monomer was prepared from 40 % aqueous solution after one night pumping to eliminate most of the water using the method describe in Talukdar et al. (2011) with minor modifications. Cold fingers containing pure samples of un-polymerized glyoxal or methyl glyoxal were temporarily kept at liquid nitrogen temperatures prior to experimental use. Glyoxal and methyl glyoxal were introduced into the chamber by passing a small flow of nitrogen through a gently warmed cold-trap.

3 Results

The data from all instruments was analyzed by the individual groups and then correlations were calculated with respect to CE-DOAS for the data from NCAR and between each instrument pair for the EUPHORE experiments. In order to account for differences in time resolution between different instruments the data points were averaged to the longest time interval of any given instrument pair (see Table 3 for time resolution of the instruments), and data points a few minutes after injection periods were removed to avoid any effects due to the instruments sampling unmixed gas from the chamber. Correlations were calculated in IGOR Pro (Wavemetrics) using the optimal distance regression (ODR) function, to account for uncertainty along both axes (y-y regression).

3.1 NCAR

The CE-DOAS, PTR-ToF-MS and FTIR instruments at NCAR used independent sources of calibration, and provide an opportunity to assess our understanding of the underlying absorption cross-section data at UV-visible and IR wavelengths, as well as

AMTD

7, 8581–8642, 2014

Instrument inter-comparison of glyoxal, methyl glyoxal and NO₂

R. Thalman et al.

Title Page

Abstract

Introduction

Conclusions

References

Tables

Figures

◀

▶

◀

▶

Back

Close

Full Screen / Esc

Printer-friendly Version

Interactive Discussion



that concentrations were high enough to obtain good signal, and the methyl glyoxal and NO₂ absorption are well separated at IR wavelengths. No significant deviations in methyl glyoxal were observed in CE-DOAS and BBCEAS, and excellent agreement is observed even in excess of 200 ppbv NO₂ (see Fig. S5 in the Supplement). We quantify the bias of 5.3 ppbv methyl glyoxal as ±1 ppbv methyl glyoxal in the presence of 200 ppbv NO₂ (or 5 pptv methyl glyoxal/1 ppbv NO₂; see Fig. 6).

3.2.3 Dry photochemical smog systems

Experiment E3 investigated *o*-xylene photo-oxidation by OH radicals in the presence of NO_x, as a source for highly variable concentrations of glyoxal, methyl glyoxal, biacetyl and NO₂ that are present simultaneously in the chamber. Figure 7 illustrates the time series, and correlation plots, and Table 3 gives the results of regression fits (correlation plots include data from before and after HONO addition and chamber opening). The slopes varied between 0.83–1.1 (glyoxal), 0.86–1.7 (methyl glyoxal), and 0.95–1.01 (NO₂), and most instruments agreed within 12, 30, and 5 %, respectively. These differences were similar or slightly larger than those observed in the pure compound experiments (Sects. 3.2.1, and 3.2.2.). Notably, differences of up to 8 % between BBCEAS and CE-DOAS for methyl glyoxal are observed despite excellent agreement (better than 1 %) for both glyoxal and NO₂. While Mad-LIP data show excellent correlation ($R^2 > 0.95$ for both α -dicarbonyls, Table 3) they also mark the largest (1.66 methyl glyoxal) and smallest (0.83 glyoxal) slopes for both α -dicarbonyls. Although FTIR performed well for methyl glyoxal, concentrations of glyoxal were close to the detection limit of the FTIR, and the measured concentrations did not scatter around zero as expected (Fig. 7a) most probably due to unknown interfering products formed because the chamber was exposed to light (ozone and HCHO formation were observed from walls). Hence, FTIR data were only considered for further discussion if values exceeded detection limits by at least a factor of 2.

In the isoprene/NO_x system (Exp. E7) results were generally similar. However, the variations in slopes were somewhat higher, i.e., 0.94–1.54 (glyoxal), and 0.7–2.2

Instrument inter-comparison of glyoxal, methyl glyoxal and NO₂

R. Thalman et al.

Title Page

Abstract

Introduction

Conclusions

References

Tables

Figures



Back

Close

Full Screen / Esc

Printer-friendly Version

Interactive Discussion



IUPAC recommendation). The chamber was left filled with 200 ppbv of O₃, acetylene (20 ppmv) was added and TME was to be injected into the chamber (with the chamber roof closed). However, before the TME could be injected, rapid glyoxal production ensued with the glyoxal concentration reaching 45 ppbv before the chamber was flushed clean (see Fig. S1 in the Supplement). The glyoxal is thought to have come from the reaction of O₃ with an impurity in the C₂H₂ (since several ppmv of C₂H₂ were added to the chamber an impurity with a relatively moderate yield of glyoxal would only have need to be 1 % of the C₂H₂ added). Several of these impurities were detected by FTIR including 60 ppbv of ethene and 160 ppbv of acetone. The ozonolysis of ethene produces OH and likely then reacted with acetylene, which produces glyoxal as well as regenerates OH.

3.2.6 Determination of precision and detection limits

Experiment 8b investigated the precision and detection limits of the various instruments by the injection of ~ 60 ppbv of glyoxal followed by an overnight flush of the chamber (4000 lpm flush rate) with all of the instruments measuring continuously in their normal operating set up until the following morning. A time series of the data is shown in Fig. S2 as part of the Supplement. Experiment E8b allowed for the acquisition of several hours of data in a clean chamber. From these baseline data (02:00 to 06:00 UTC) histograms were calculated for each of the instruments with available data. A Gaussian function was fitted to the histograms except in the case of the FT-IR, where the spread of data did not form a Gaussian distribution and instead a simple average and standard deviation were calculated.

From the Gaussian distribution the standard deviation and mean were calculated for each instrument (see Fig. 9 for glyoxal and Fig. 10 for methyl glyoxal, also using data from Exp. E8b). The limit of detection (LOD) is defined as follows:

$$\text{LOD}_{\text{exp}} = 3 \cdot \sigma_{\text{Gaussian}} \quad (7)$$

Instrument inter-comparison of glyoxal, methyl glyoxal and NO₂

R. Thalman et al.

Title Page

Abstract

Introduction

Conclusions

References

Tables

Figures

◀

▶

◀

▶

Back

Close

Full Screen / Esc

Printer-friendly Version

Interactive Discussion



of 3% uncertainty for absorption cross-sections at the visible and IR spectral ranges (Volkamer et al., 2005b).

Measurements of methyl glyoxal in this study are calibrated using an integrated IR cross-section of 7.88×10^{-18} cm molecule⁻¹ near 2830 cm⁻¹ to calibrate the EUPHORE FTIR, and 2.58×10^{-17} cm molecule⁻¹ near 1740 cm⁻¹ to calibrate the NCAR FTIR. Direct comparison of the EUPHORE and NCAR IR spectra showed a factor of 0.78 difference, which was traced to a near identical correction factor that had previously been applied to the EUPHORE-IR spectrum (see Sect. 2.1.8). This factor comes from the use of an older cross-section (Raber, 1992) and cross-calibration with the WDOAS system. We note that the NCAR IR cross-section spectrum is 4% lower than the IR cross-section measured at Pacific Northwest National Laboratory (PNNL) (Profeta et al., 2011), and further agrees well with other studies (Raber, 1992; Talukdar et al., 2011). After re-normalization (eliminating the factor 0.78) the EUPHORE IR spectrum agrees well with the other IR spectra (Profeta et al., 2011; Talukdar et al., 2011). Further, the NCAR experiments provide a first temperature dependent cross-calibration of the vis- and IR spectral ranges for methyl glyoxal. The correlations for NCAR experiments find no evidence for a temperature effect, and slopes are unity with 1% error. The vis spectrum by Meller et al. (1991) results in a near identical calibration for CE-DOAS as the above integral IR cross section for the NCAR FTIR. Finally, ion-molecule rate constant calculations for the reaction of methyl glyoxal with H₃O⁺ result in slopes between PTR-ToF-MS and CE-DOAS of 0.95 ± 0.03 ; this is essentially unity at the 95% confidence level. Six independent sources of calibration are therefore consistent within 5%, which we interpret as an upper limit for the uncertainty in the vis- and IR cross sections of methyl glyoxal, and as the uncertainty in the ion-molecule rate constant ($\text{rate} = 1.47 \times 10^{-9}$ cm³ s⁻¹). Based on the comprehensive evidence we recommend the following integrated IR cross-section values for use in future studies: 3.0×10^{-17} cm molecule⁻¹ near 1740 cm⁻¹; 9.9×10^{-18} cm molecule⁻¹ near 2830 cm⁻¹.

Instrument inter-comparison of glyoxal, methyl glyoxal and NO₂

R. Thalman et al.

Title Page

Abstract

Introduction

Conclusions

References

Tables

Figures

◀

▶

◀

▶

Back

Close

Full Screen / Esc

Printer-friendly Version

Interactive Discussion



4.2 Precision, accuracy, and limit of detection

The methods underlying determination of detection limits for instruments compared in this study differ, and hence values reported for limit of detection, LOD, in the literature are not easily comparable. The simultaneous observation of the same air mass provides an opportunity to calculate LOD using a consistent definition, i.e., $\text{LOD} = 3 \cdot 1\text{-}\sigma$ variability + background. Here “variability” is assessed during a period when the sensor signal is expected to be constant. This definition represents the only way to define LOD for single-channel instruments (e.g. fluorescence, chemiluminescence, phosphorescence, and voltammetry), and is widely used in analytical chemistry (IUPAC, 2006). It also is closely related to the fit-error from spectral fitting of multi-channel detectors. These multi-channel sensors, however, can leverage additional information (channels, through spectral fitting) to define LOD, for example, accounting for systematic residual structures that may remain after all known absorbers have been accounted for. Such structures – if present – inform on the potential for systematic bias due to spectral cross-correlation (see Sect. 4 in Thalman and Volkamer, 2010). Any deviation from pure white-noise residuals can be accessed from multi-channel sensors, and provides additional information to assess LOD from a perspective of “accuracy”. These different definitions can lead to a factor of 6 difference between notations for LOD numbers reported in the literature (Stutz and Platt, 1996; Thalman and Volkamer, 2010).

We used Eq. (7) to calculate experimental LODs using the $1\text{-}\sigma$ variability of data from the overnight dilution experiment on 5–6 July 2011 (E8b; see Fig. S2 in the Supplement). These experimental LODs are listed together with LOD values submitted with their measurement data by the operators of the various instruments. We find excellent agreement between the experimental LODs determined here and the reported LODs, once a common definition is applied. As seen in Figs. 9 and 10, the distributions are Gaussian (except for FTIR) and yielded LODs lower than or similar to the values reported for each instrument (see Table 4). All instruments performed within their specifications.

Instrument inter-comparison of glyoxal, methyl glyoxal and NO_2

R. Thalman et al.

Title Page

Abstract

Introduction

Conclusions

References

Tables

Figures



Back

Close

Full Screen / Esc

Printer-friendly Version

Interactive Discussion



Instrument inter-comparison of glyoxal, methyl glyoxal and NO₂

R. Thalman et al.

Title Page

Abstract

Introduction

Conclusions

References

Tables

Figures



Back

Close

Full Screen / Esc

Printer-friendly Version

Interactive Discussion



For the Mad-LIP instrument problems caused by the initially low flows prevented noticing that the multi-pass optics in the LIP cell were degraded. Testing after the field campaign confirmed that mirror degradation had a two-fold effect in that the background scatter was increased and the effective laser-power reduced. Both factors reduce the LOD explaining the difference between the LOD reported in Henry et al. (2012) and the value in Table 4. The variability of the slope of the LIP instrument is attributed to alignment variations of the multi-pass cell. Changes in alignment affect the net laser power in the detection volume and are hard to account for. Such alignment changes resulted from the instrument maintenance performed during the intercomparison as part of the diagnostics of the flow problems and the low detection limit. Based on the results of this intercomparison a new version of Mad-LIP is using a single-cell detection axis with comparable detection efficiency but much greater stability (as demonstrated for LIF measurement of formaldehyde (Keutsch and Wolfe, 2014)).

Assessing the accuracy of an instrument is not possible without comparison to other instruments. Accuracy represents the measurement uncertainty at high signal to noise (see Ryerson et al. (2013), Thalman and Volkamer, 2010). We assess it from the variability in slopes relative to CE-DOAS, using only data from experiments where the maximum concentration is at least 10 times larger than the 1- σ variability deduced from the overnight dilution experiment (LOQ, limit of quantification). We note that all instruments during EUPHORE experiments were either calibrated directly or indirectly from the same UV-visible cross-section (Volkamer et al., 2005b). This calibration is directly accomplished by fitting the convoluted literature cross-sections for W-DOAS, CE-DOAS and BBCEAS. Calibration is less direct for FTIR (cross-section calibrated to the W-DOAS, SPME calibrated to the FTIR). Mad-LIP is calibrated by flowing a calibration gas through a ring-down cell monitoring the 440 nm absorption feature, and into the LIP instrument; UV-visible absorption by the ring-down cell is calibrated from the glyoxal or methyl glyoxal UV-visible cross-section. By relating all instruments to a common source of calibration information the experiments at EUPHORE eliminate potential for calibration bias, and isolate other (unknown) factors that may limit accuracy.

**Instrument
inter-comparison of
glyoxal, methyl
glyoxal and NO₂**

R. Thalman et al.

Title Page

Abstract

Introduction

Conclusions

References

Tables

Figures



Back

Close

Full Screen / Esc

Printer-friendly Version

Interactive Discussion



The observed variability in slopes between experiments is usually larger than the uncertainty in the cross-section (see Sect. 4.1.). The 95 % confidence intervals of slopes are listed in Table 4 for all instruments (relative to CE-DOAS) as a measure of accuracy at high signal-to-noise. This was done by averaging these slopes relative to CE-DOAS for each instrument and assessing the confidence interval of this sample of slopes (thus omitting experiments where the correlation does not include a maximum value of at least $10 \times$ the 1-sigma detection limit). It is generally smallest (4–7 %) for instruments which benefit from direct calibration, and larger for Mad-LIP (glyoxal: average slope = 1.06 ± 0.53 ; methyl glyoxal: average slope = 1.80 ± 0.58), and SPME (glyoxal: average slope = 1.14 ± 0.53 ; methyl glyoxal: average slope = 0.75 ± 0.18) and PTR-ToF-MS (1.23, only one measurement).

We chose CE-DOAS to assess relative differences to other instruments for the following reasons: (1) the instrument participated in both campaigns, (2) had excellent data coverage, and (3) high time resolution. Use of CE-DOAS yields the maximum number of data points to calculate correlations between different instruments at EUPHORE. Further, (4) CE-DOAS demonstrated the lowest LOD for both glyoxal and methyl glyoxal among all available instruments (see Table 4); (5) CE-DOAS benefits from inherent path length calibration through O₄ at very high signal-to-noise to demonstrate control over cavity alignment with very little error (2 %). Both CE-DOAS and BBCEAS fit most of these criteria but ultimately CE-DOAS was chosen as the reference technique to tie the two separate measurement exercises together. The comprehensive coverage and consistent performance from CE-DOAS in context with the other instruments that we compared at both chamber facilities provides strong evidence to suggest CE-DOAS is precise, and accurate. The Supplement contains a discussion of potential sources for systematic bias with CE-DOAS measurements. The resulting error of 3.5 % is dominated by the uncertainty in the absorption cross-sections, and further information is provided in the Supplement, and Fig. S4 in the Supplement.

4.3 Interference from biacetyl and O₃

Biacetyl is formed simultaneously with glyoxal and methyl glyoxal in a complex array of other ring opening and retaining products in the photo-oxidation of *o*-xylene. We did not observe any measurable interference in detection of glyoxal and methyl glyoxal from biacetyl up to ~2 ppbv (estimated from model simulation of the chamber reaction and known yields) during Experiment E3. Most instrument slopes agreed within 10% for glyoxal, and differences of ~20% for Mad-LIP cannot be explained by biacetyl signals, which would result in larger than unity slopes. BBCEAS, CE-DOAS and W-DOAS are expected to be insensitive to interference from biacetyl, due to its relatively unstructured absorption cross-section (see Fig. S4 in the Supplement) and the fact that the selectivity of retrievals arises from differential absorption structures (prominent for glyoxal). Similarly, sensitivity for biacetyl by Mad-LIP had been tested previously and the lack of sensitivity (no phosphorescence) due to quenching by oxygen is consistent with findings in this study (Henry et al., 2012).

The hypothesis for this experiment was that the structure of the biacetyl absorption cross-section (Fig. S3 in the Supplement) could cause interferences for other α -dicarbonyls. For methyl glyoxal, BBCEAS and SPME during Exp. E3 were 8 and 13% respectively lower than CE-DOAS, while FTIR and Mad-LIP showed slopes that were 30% and 70% higher. For FTIR, this positive bias appears to be twice as high as during Experiment E2, the only other methyl glyoxal comparison available. We note that methyl glyoxal concentrations of 8 and 12 ppbv for FTIR and Mad-LIP (see Fig. 7), respectively, during Exp. E3 are only 2–3 times above the FTIR detection limit. Thus the difference of 15% compared to Exp. E2 can probably (at least) partially explained by systematic bias of FTIR near the detection limit as well as the complex mixture in the chamber for photo-oxidation experiments including the incomplete subtraction of water bands in the FTIR. SOA formation is unlikely to affect the optical measurements; scattering is inefficient at IR wavelengths, and a filter removes SOA in the CE-DOAS sampling line. The positive difference in slope observed for Mad-LIP currently remains

AMTD

7, 8581–8642, 2014

Instrument inter-comparison of glyoxal, methyl glyoxal and NO₂

R. Thalman et al.

Title Page

Abstract

Introduction

Conclusions

References

Tables

Figures



Back

Close

Full Screen / Esc

Printer-friendly Version

Interactive Discussion



**Instrument
inter-comparison of
glyoxal, methyl
glyoxal and NO₂**

R. Thalman et al.

Title Page

Abstract

Introduction

Conclusions

References

Tables

Figures

◀

▶

◀

▶

Back

Close

Full Screen / Esc

Printer-friendly Version

Interactive Discussion

uncertainty in the measurements. The primary effects of high NO₂ (> 10 ppbv) are due to NO₂ light extinction. This limits the attainable effective absorption path lengths, and removes photons, thus further increasing photon shot noise as well as the effects of the differential absorption structure. All of these effects lead to increasing uncertainty for measured glyoxal and methyl glyoxal. For the CE-DOAS ($R = 0.999972$) 200 ppbv of NO₂ changes the sample path length from 15 to 3.5 km and the light throughput is reduced by a factor 4. The combined effect is a decrease of a factor of 16 in sensitivity. For BBCEAS the effects are similar, but the reduction in path length is from 5–2.3 km (a factor of 2). At the highest level of NO₂ (~ 200 ppbv) the absorption due to NO₂ is more than 500 times greater than that due to 0.3 ppbv of glyoxal and more than 300 times greater than for 6 ppbv of methyl glyoxal. The largest effect of the NO₂ is differential absorption structure of the NO₂ is to create residual structures (both in absorption and as the wavelength dependent path length begins to follow the structure of the NO₂ extinction) that make DOAS retrievals difficult for all of the visible light absorption techniques (W-DOAS, CE-DOAS and BBCEAS) as well creating a highly structured absorption path length in the cavity based instruments (CE-DOAS and BBCEAS). For instance, the variation in the absorption path length for CE-DOAS is 35 % over the space of 3 nm with 200 ppbv of NO₂ in the instrument. Despite this difference in the differential absorption, the very small biases in glyoxal and methyl glyoxal due to NO₂ is indeed surprising, and encouraging. The Mad-LIP glyoxal measurements are unaffected by large amounts of NO₂. The FTIR showed a slight increase in the methyl glyoxal signal relative to the SF₆ tracer (Fig. 6). The W-DOAS instrument may be similarly affected by large fitting residuals due to NO₂, but the range of glyoxal used in the experiment was below the detection limit for the instrument, as was the FTIR for the glyoxal experiment and the Mad-LIP was off-line for the methyl glyoxal experiment. For the SPME the reported concentrations varied too widely to evaluate the interference.

4.5 Relevance for α -dicarbonyl measurements in the atmosphere

Our results show that advances with measurement techniques in recent years are suitable to attempt the detection of glyoxal at ambient mixing ratios in urban, semi-polluted, biogenic, arctic and marine environments. In most urban environments the glyoxal detection by in situ UV-vis absorption techniques is feasible, i.e., there is no fundamental limitation due to typical ambient NO_2 concentrations. However, care must be taken with accurately characterizing the effect of NO_2 on the effective absorption paths, and the representation of overlapping absorption features during retrievals. Several optical techniques now facilitate the fast (few Hz) in situ detection of glyoxal. Such time resolution is suitable to conduct measurements from mobile platforms such as aircraft, or for micro-meteorological flux calculations. The first Eddy Covariance Flux measurements of glyoxal have recently been demonstrated by CE-DOAS over the remote ocean (Coburn et al., 2014).

Measurements of methyl glyoxal in the atmosphere are complicated by a short atmospheric lifetime ($\sim 0.5\text{--}1$ h). As a result, ambient mixing ratios are comparable and often lower than those of glyoxal. Detection by optical absorption techniques at UV-vis wavelengths has limited sensitivity since the absorption cross-section of methyl glyoxal is ~ 10 times lower compared to glyoxal; at IR wavelength the combination of low cross-sections and spectral overlap with other species complicates measurements of low ambient concentrations. Detection by phosphorescence is complicated by significant interferences from glyoxal that renders calibration factors too strong a function of environmental conditions to facilitate a meaningful quantification of methyl glyoxal in the presence of glyoxal. Detection by PTR-ToF-MS has the issue of coincidental masses from reaction intermediates and the fragmentation of larger compounds upon protonation in the mass spectrometer. There still remains a need to develop highly time-resolved on-line measurements of methyl glyoxal at ambient mixing ratio levels.

AMTD

7, 8581–8642, 2014

Instrument inter-comparison of glyoxal, methyl glyoxal and NO_2

R. Thalman et al.

Title Page

Abstract

Introduction

Conclusions

References

Tables

Figures

◀

▶

◀

▶

Back

Close

Full Screen / Esc

Printer-friendly Version

Interactive Discussion



5 Conclusions

During two separate inter-comparison campaigns nine instruments that measured α -dicarbonyls were compared (3 at NCAR, 7 at EUPHORE; CE-DOAS participated in both campaigns). The nine instruments used three independent sources of calibration (see Sect. 4.1), and additional comparisons with calibrations of literature cross-section data were conducted. Systematic bias between techniques was eliminated by observing the same air volume, and calibration bias was minimized as far as possible by relating the calibrations of most instruments at EUPHORE (except the PTR-ToF-MS for methyl glyoxal) to the UV-vis absorption cross-sections. We conclude:

1. The absorption cross-section spectra for glyoxal and methyl glyoxal at Vis and IR wavelengths are robust. Simultaneous measurements at vis and IR wavelengths agree within $2 \pm 3\%$ for glyoxal, and within $1 \pm 4\%$ for methyl glyoxal. No evidence is found for a temperature effect over the range from 293 K to 330 K in either glyoxal or methyl glyoxal cross-sections. Further, the NCAR PTR-ToF-MS calibration based on a theoretical calculation of the proton affinity of methyl glyoxal agrees with visible and IR calibrations within 5%.
2. Seven instruments at EUPHORE used a common source for calibration from the same UV-visible spectrum for glyoxal (Volkamer et al., 2005b) and methyl glyoxal (Meller et al., 1991). We find excellent linearity between all instruments under idealized conditions (pure glyoxal or methyl glyoxal, $R^2 > 0.96$), and in complex gas mixtures characteristic of dry photochemical smog systems (*o*-xylene/ NO_x and isoprene/ NO_x , $R^2 > 0.95$; $R^2 \sim 0.65$ for offline SPME measurements of methyl glyoxal). The correlations are slightly more variable in humid ambient air mixtures ($\text{RH} > 45\%$) for methyl glyoxal ($0.58 < R^2 < 0.68$) than for glyoxal ($0.79 < R^2 < 0.99$).
3. The intercepts of correlations were largely found to be insignificant (below experimentally determined detection limits), and slopes varied by less than 5% for NO_2 .

AMTD

7, 8581–8642, 2014

Instrument inter-comparison of glyoxal, methyl glyoxal and NO_2

R. Thalman et al.

Title Page

Abstract

Introduction

Conclusions

References

Tables

Figures



Back

Close

Full Screen / Esc

Printer-friendly Version

Interactive Discussion



The Supplement related to this article is available online at
doi:10.5194/amtd-7-8581-2014-supplement.

Acknowledgements. This work was supported by Eurochamp II project E2-2011-03-07-0054, Instituto Universitario CEAM-UMH, and the National Science Foundation. The Instituto Universitario CEAM-UMH is partly supported by Generalitat Valenciana, and the projects GRACCIE (Consolider-Ingenio 2010) and FEEDBACKS (Prometeo – Generalitat Valenciana). EUPHORE instrumentation is partly funded by the Spanish Ministry of Science and Innovation, through INNPLANTA project: PCT-440000-2010-003. The National Center for Atmospheric Research is operated by the University Corporation for Atmospheric Research, under the sponsorship of the National Science Foundation. R. Thalman acknowledges consecutive graduate fellowships from NASA and CIRES. R. Volkamer acknowledges financial support from NSF-AGS CAREER award ATM-0847793, and CU Boulder start-up funds. R. Seco was partially supported by a postdoctoral grant from Fundación Ramón Areces. M. J. S. Daniels and I. C. A. Goodall were supported on Ph.D. studentships sponsored by the UK's Natural Environment Research Council. University of Leeds and Leicester participants were supported by the UK National Environmental Research Council (NERC). A. R. Rickard, M. T. Baeza-Romero and P. S. Monks gratefully acknowledge the support of the UK Natural Environment Research Council for funding of the PhoSOA project (NE/H021108/1). A. R. Rickard and S. M. Ball also acknowledge financial and logistical support from the NERC National Centre for Atmospheric Science-Composition.

References

- Ahlm, L., Liu, S., Day, D. A., Russell, L. M., Weber, R., Gentner, D. R., Goldstein, A. H., DiGangi, J. P., Henry, S. B., Keutsch, F. N., VandenBoer, T. C., Markovic, M. Z., Murphy, J. G., Ren, X., and Scheller, S.: Formation and growth of ultrafine particles from secondary sources in Bakersfield, California, *J. Geophys. Res.*, 117, D00V08, doi:10.1029/2011JD017144, 2012.
- Alvarez, E. G. and Valcárcel, M.: Research into conditions of quantity in the determination of carboniles in complex air matrices by adsorptive solid phase microextraction, *Talanta*, 77, 1444–1453, 2009

AMTD

7, 8581–8642, 2014

Instrument inter-comparison of glyoxal, methyl glyoxal and NO₂

R. Thalman et al.

Title Page

Abstract

Introduction

Conclusions

References

Tables

Figures

⏪

⏩

◀

▶

Back

Close

Full Screen / Esc

Printer-friendly Version

Interactive Discussion



**Instrument
inter-comparison of
glyoxal, methyl
glyoxal and NO₂**

R. Thalman et al.

Title Page

Abstract

Introduction

Conclusions

References

Tables

Figures



Back

Close

Full Screen / Esc

Printer-friendly Version

Interactive Discussion

Kim, S., Nakashima, Y., Wolfe, G. M., Kajii, Y., Apel, E.C., Goldstein, A. H., Guenther, A., Karl, T., Hansel, A., and Keutsch, F. N.: Observations of glyoxal and formaldehyde as metrics for the anthropogenic impact on rural photochemistry, *Atmos. Chem. Phys.*, 12, 9529–9543, doi:10.5194/acp-12-9529-2012, 2012.

5 Dubé, W. P., Brown, S. S., Osthoff, H. D., Nunley, M. R., Ciciora, S. J., Paris, M. W., McLaughlin, R. J., and Ravishankara, A. R.: Aircraft instrument for simultaneous, in situ measurement of NO₃ and N₂O₅ via pulsed cavity ring-down spectroscopy, *Rev. Sci. Instrum.*, 77, 034101–034111, 2006.

10 Ervens, B. and Volkamer, R.: Glyoxal processing by aerosol multiphase chemistry: towards a kinetic modeling framework of secondary organic aerosol formation in aqueous particles, *Atmos. Chem. Phys.*, 10, 8219–8244, doi:10.5194/acp-10-8219-2010, 2010.

Ervens, B., Carlton, A. G., Turpin, B. J., Altieri, K. E., Kreidenweis, S. M., and Feingold, G.: Secondary organic aerosol yields from cloud-processing of isoprene oxidation products, *Geophys. Res. Lett.*, 35, L02816, doi:10.1029/2007GL031828, 2008.

15 Fayt, C. and Van Roosendael, M.: WinDOAS User Manual, Belgian Institute for Space Aeronomy, Brussels, Belgium, 2001.

Feierabend, K. J., Zhu, L., Talukdar, R. K., and Burkholder, J. B.: Rate coefficients for the OH + HC(O)C(O)H (glyoxal) reaction between 210 and 390 K, *J. Phys. Chem. A*, 112, 73–82, 2007.

20 Fu, T. M., Jacob, D. J., Wittrock, F., Burrows, J. P., Vrekoussis, M., and Henze, D. K.: Global budgets of atmospheric glyoxal and methylglyoxal, and implications for formation of secondary organic aerosols, *J. Geophys. Res.*, 113, D15303, doi:10.1029/2007JD009505, 2008.

Galloway, M. M., Chhabra, P. S., Chan, A. W. H., Surratt, J. D., Flagan, R. C., Seinfeld, J. H., and Keutsch, F. N.: Glyoxal uptake on ammonium sulphate seed aerosol: reaction products and reversibility of uptake under dark and irradiated conditions, *Atmos. Chem. Phys.*, 9, 3331–3345, doi:10.5194/acp-9-3331-2009, 2009.

25 Gómez Alvarez, E., Viidanoja, J., Muñoz, A., Wirtz, A., and Hjorth, J.: Experimental confirmation of the dicarbonyl route in the photo-oxidation of toluene and benzene, *Environ. Sci. Technol.*, 41, 8362–8369, doi:10.1021/es0713274, 2007.

30 Grosjean, E., Grosjean, D., Fraser, M. P., and Cass, G. R.: Air quality model evaluation data for organics. 2. C1–C14 Carbonyls in Los Angeles air, *Environ. Sci. Technol.*, 30, 2687–2703, 1996.



**Instrument
inter-comparison of
glyoxal, methyl
glyoxal and NO₂**

R. Thalman et al.

Title Page

Abstract

Introduction

Conclusions

References

Tables

Figures

◀

▶

◀

▶

Back

Close

Full Screen / Esc

Printer-friendly Version

Interactive Discussion



- Ip, H. S. S., Huang, X. H. H., and Yu, J. Z.: Effective Henry's law constants of glyoxal, glyoxylic acid, and glycolic acid, *Geophys. Res. Lett.*, 36, L01802, doi:10.1029/2008GL036212, 2009.
- Jordan, A., Haidacher, S., Hanel, G., Hartungen, E., Märk, L., Seehauser, H., Schottkowsky, R., Sulzer, P., and Märk, T. D.: A high resolution and high sensitivity proton-transfer-reaction time-of-flight mass spectrometer (PTR-TOF-MS), *Int. J. Mass Spectrom.*, 286, 122–128, 2009.
- Kampf, C. J., Waxman, E. M., Slowik, J. G., Dommen, J., Pfaffenberger, L., Praplan, A. P., Prévôt, A. S. H., Baltensperger, U., Hoffmann, T., and Volkamer, R.: Effective Henry's law partitioning and the salting constant of glyoxal in aerosols containing sulfate, *Environ. Sci. Technol.*, 47, 4236–4244, 2013.
- Keutsch, F. N. and Wolfe, G. M.: In situ Airborne Formaldehyde (ISAF) for CONTRAST 2014, available at: http://www2.acd.ucar.edu/sites/default/files/contrast/ISAF_Instrumentbrief.pdf (last access: 1 July 2014), 2014.
- Karl, T., Guenther, A., Turnipseed, A., Tyndall, G., Artaxo, P., and Martin, S.: Rapid formation of isoprene photo-oxidation products observed in Amazonia, *Atmos. Chem. Phys.*, 9, 7753–7767, doi:10.5194/acp-9-7753-2009, 2009.
- Langridge, J. M., Ball, S. M., Shillings, A. J. L., and Jones, R. L.: A broadband absorption spectrometer using light emitting diodes for ultrasensitive, in situ trace gas detection, *Rev. Sci. Instrum.*, 79, 123110, doi:10.1063/1.3046282, 2008.
- McNeill, V. F., Woo, J. L., Kim, D. D., Schwier, A. N., Wannell, N. J., Sumner, A. J., and Barakat, J. M.: Aqueous-phase secondary organic aerosol and organosulfate formation in atmospheric aerosols: a modeling study, *Environ. Sci. Technol.*, 46, 8075–8081, 2012.
- Meller, R., Raber, W., Crowley, J. N., Jenkin, M. E., and Moortgat, G. K.: The UV-visible absorption spectrum of methylglyoxal, *J. Photoch. Photobio. A*, 62, 163–171, 1991.
- Michel, E., Schoon, N., Amelynck, C., Guimbaud, C., Catoire, V., and Arijs, E.: A selected ion flow tube study of the reactions of H₃O⁺, NO⁺ and O₂⁺ with methyl vinyl ketone and some atmospherically important aldehydes, *Int. J. Mass Spectrom.*, 244, 50–59, 2005.
- Muñoz, A., Vera, T., Sidebottom, H., Mellouki, A., Borrás, E., Rodenas, M., Clemente, E., and Vazquez, M.: Studies on the atmospheric degradation of chlorpyrifosmethyl, *Environ. Sci. Technol.*, 45, 1880–1886, 2011.
- Muñoz, A., Vera, T., Sidebottom, H., Ródenas, M., Borrás, E., Vázquez, M., Raro, M., and Mellouki, A.: Studies on the atmospheric fate of propachlor (2-chloro-Nisopropylacetanilide) in the gas-phase, *Atmos. Environ.*, 49, 33–40, 2012.

**Instrument
inter-comparison of
glyoxal, methyl
glyoxal and NO₂**

R. Thalman et al.

Title Page

Abstract

Introduction

Conclusions

References

Tables

Figures



Back

Close

Full Screen / Esc

Printer-friendly Version

Interactive Discussion



Rodenas, M.: Improvements in Spectroscopy Data Processing: Faster Production and Better Reliability of Laboratory Data, Report for ESF-INTROP Exchange Grants, available at: <http://www.ceam.es/GVAceam/archivos/MRodenasiINTROPReport.pdf> (last access: 18 August 2014), 2008.

5 Rothman, L. S., Gordon, I. E., Barbe, A., Benner, D. C., Bernath, P. F., Birk, M., Boudon, V., Brown, L. R., Campargue, A., Champion, J. P., Chance, K., Coudert, L. H., Dana, V., Devi, V. M., Fally, S., Flaud, J. M., Gamache, R. R., Goldman, A., Jacquemart, D., Kleiner, I., Lacombe, N., Lafferty, W. J., Mandin, J. Y., Massie, S. T., Mikhailenko, S. N., Miller, C. E., Moazzen-Ahmadi, N., Naumenko, O. V., Nikitin, A. V., Orphal, J., Perevalov, V. I., Perrin, A., Predoi-Cross, A., Rinsland, C. P., Rotger, M., Simeckov, M., Smith, M. A. H., Sung, K., Tashkun, S. A., Tennyson, J., Toth, R. A., Vandaele, A. C., and Vander Auwera, J.: The HITRAN 2008 molecular spectroscopic database, *J. Quant. Spectrosc. Ra.*, 110, 533–572, 2009.

15 Ryerson, T. B., Andrews, A. E., Angevine, W. M., Bates, T. S., Brock, C. A., Cairns, B., Cohen, R. C., Cooper, O. R., de Gouw, J. A., Fehsenfeld, F. C., Ferrare, R. A., Fischer, M. L., Flagan, R. C., Goldstein, A. H., Hair, J. W., Hardesty, R. M., Hostetler, C. A., Jimenez, J. L., Langford, A. O., McCauley, E., McKeen, S. A., Molina, L. T., Nenes, A., Oltmans, S. J., Parrish, D. D., Pederson, J. R., Pierce, R. B., Prather, K., Quinn, P. K., Seinfeld, J. H., Senff, C. J., Sorooshian, A., Stutz, J., Surratt, J. D., Trainer, M., Volkamer, R., Williams, E. J., and Wofsy, S. C.: The 2010 California research at the Nexus of air quality and climate change (CalNex) field study, *J. Geophys. Res.*, 5830–5866, doi:10.1002/jgrd.50331, 2013.

Shetter, R. E., Davidson, J. A., Cantrell, C. A., and Calvert, J. G.: Temperature variable long path cell for absorption-measurements, *Rev. Sci. Instrum.*, 58, 1427–1428, 1987.

25 Sinreich, R., Volkamer, R., Filsinger, F., Frieß, U., Kern, C., Platt, U., Sebastián, O., and Wagner, T.: MAX-DOAS detection of glyoxal during ICARTT 2004, *Atmos. Chem. Phys.*, 7, 1293–1303, doi:10.5194/acp-7-1293-2007, 2007.

Stavrakou, T., Müller, J.-F., De Smedt, I., Van Roozendaal, M., Kanakidou, M., Vrekoussis, M., Wittrock, F., Richter, A., and Burrows, J. P.: The continental source of glyoxal estimated by the synergistic use of spaceborne measurements and inverse modelling, *Atmos. Chem. Phys.*, 9, 8431–8446, doi:10.5194/acp-9-8431-2009, 2009.

30 Talukdar, R. K., Zhu, L., Feierabend, K. J., and Burkholder, J. B.: Rate coefficients for the reaction of methylglyoxal (CH₃COCHO) with OH and NO₃ and glyoxal (HCO)₂ with NO₃, *Atmos. Chem. Phys.*, 11, 10837–10851, doi:10.5194/acp-11-10837-2011, 2011.

Instrument inter-comparison of glyoxal, methyl glyoxal and NO₂

R. Thalman et al.

Title Page

Abstract

Introduction

Conclusions

References

Tables

Figures



Back

Close

Full Screen / Esc

Printer-friendly Version

Interactive Discussion



Thalman, R. and Volkamer, R.: Inherent calibration of a blue LED-CE-DOAS instrument to measure iodine oxide, glyoxal, methyl glyoxal, nitrogen dioxide, water vapour and aerosol extinction in open cavity mode, *Atmos. Meas. Tech.*, 3, 1797–1814, doi:10.5194/amt-3-1797-2010, 2010.

5 Thalman, R., Zarzana, K. J., Tolbert, M. A., and Volkamer, R.: Rayleigh scattering cross-section measurements of nitrogen, argon, oxygen and air, *J. Quant. Spectrosc. Ra.*, 147, 171–177, 2014.

Topping, D., Connolly, P., and McFiggans, G.: Cloud droplet number enhanced by co-condensation of organic vapours, *Nat. Geosci.*, 6, 443–446, 2013.

10 Tuazon, E. C. and Atkinson, R.: A product study of the gas-phase reaction of isoprene with the OH radical in the presence of NO_x, *Int. J. Chem. Kinet.*, 22, 1221–1236, 1990a.

Tuazon, E. C. and Atkinson, R.: A product study of the gas-phase reaction of Methacrolein with the OH radical in the presence of NO_x, *Int. J. Chem. Kinet.*, 22, 591–602, 1990b.

15 Vandaele, A. C., Hermans, C., Fally, S., Carleer, M., Colin, R., Merienne, M. F., Jenouvrier, A., and Coquart, B.: High-resolution Fourier transform measurement of the NO₂ visible and near-infrared absorption cross sections: temperature and pressure effects, *J. Geophys. Res.*, 107, 4348, doi:10.1029/2001JD000971, 2002.

Volkamer, R., Molina, L. T., Molina, M. J., Shirley, T., and Brune, W. H.: DOAS measurement of glyoxal as an indicator for fast VOC chemistry in urban air, *Geophys. Res. Lett.*, 32, L08806, doi:10.1029/2005GL022616, 2005a.

20 Volkamer, R., Spietz, P., Burrows, J., and Platt, U.: High-resolution absorption cross-section of glyoxal in the UV-vis and IR spectral ranges, *J. Photoch. Photobio. A*, 172, 35–46, 2005b.

Volkamer, R., San Martini, F., Molina, L. T., Salcedo, D., Jimenez, J. L., and Molina, M. J.: A missing sink for gas-phase glyoxal in Mexico City: formation of secondary organic aerosol, *Geophys. Res. Lett.*, 34, L19807, doi:10.1029/2007GL030752, 2007.

25 Volkamer, R., Ziemann, P. J., and Molina, M. J.: Secondary Organic Aerosol Formation from Acetylene (C₂H₂): seed effect on SOA yields due to organic photochemistry in the aerosol aqueous phase, *Atmos. Chem. Phys.*, 9, 1907–1928, doi:10.5194/acp-9-1907-2009, 2009.

30 Washenfelder, R. A., Langford, A. O., Fuchs, H., and Brown, S. S.: Measurement of glyoxal using an incoherent broadband cavity enhanced absorption spectrometer, *Atmos. Chem. Phys.*, 8, 7779–7793, doi:10.5194/acp-8-7779-2008, 2008.

Washenfelder, R. A., Young, C. J., Brown, S. S., Angevine, W. M., Atlas, E. L., Blake, D. R., Bon, D. M., Cubison, M. J., de Gouw, J. A., Dusanter, S., Flynn, J., Gilman, J. B., Graus, M.,

**Instrument
inter-comparison of
glyoxal, methyl
glyoxal and NO₂**

R. Thalman et al.

Title Page

Abstract

Introduction

Conclusions

References

Tables

Figures



Back

Close

Full Screen / Esc

Printer-friendly Version

Interactive Discussion



Griffith, S., Grossberg, N., Hayes, P. L., Jimenez, J. L., Kuster, W. C., Lefer, B. L., Pollack, I. B., Ryerson, T. B., Stark, H., Stevens, P. S., and Trainer, M. K.: The glyoxal budget and its contribution to organic aerosol for Los Angeles, California, during CalNex 2010, *J. Geophys. Res.*, 116, D00V02, doi:10.1029/2011JD016314, 2011.

5 Waxman, E. M., Dzepina, K., Ervens, B., Lee-Taylor, J., Aumont, B., Jimenez, J. L., Madronich, S., and Volkamer, R.: Secondary organic aerosol formation from semi- and intermediate-volatility organic compounds and glyoxal: relevance of O/C as a tracer for aqueous multiphase chemistry, *Geophys. Res. Lett.*, 40, 978–982, 2013.

10 Wyche, K. P., Blake, R. S., Ellis, A. M., Monks, P. S., Brauers, T., Koppmann, R., and Apel, E. C.: Technical Note: Performance of Chemical Ionization Reaction Time-of-Flight Mass Spectrometry (CIR-TOF-MS) for the measurement of atmospherically significant oxygenated volatile organic compounds, *Atmos. Chem. Phys.*, 7, 609–620, doi:10.5194/acp-7-609-2007, 2007.

15 Yu, G., Bayer, A. R., Galloway, M. M., Korshavn, K. J., Fry, C. G., and Keutsch, F. N.: Glyoxal in aqueous ammonium sulfate solutions: products, kinetics and hydration effects, *Environ. Sci. Technol.*, 45, 6336–6342, 2011.

Yu, J., Jeffries, H. E., and Sexton, K. G.: Atmospheric photooxidation of alkylbenzenes – I. Carbonyl product analyses, *Atmos. Environ.*, 31, 2261–2280, 1997.

20 Zalicki, P. and Zare, R. N.: Cavity ring-down spectroscopy for quantitative absorption-measurements, *J. Chem. Phys.*, 102, 2708–2717, 1995.

Instrument inter-comparison of glyoxal, methyl glyoxal and NO₂

R. Thalman et al.

Title Page

Abstract

Introduction

Conclusions

References

Tables

Figures

◀

▶

◀

▶

Back

Close

Full Screen / Esc

Printer-friendly Version

Interactive Discussion



Table 1. Instrumentation and measured species at NCAR and EUPHORE.

Instrument ^a	Participant ^b	Location	Measured Species ^c	Measured quantity	Sample location
CE-DOAS	CU	NCAR	G, M, N	^d	Outside
NCAR FTIR	NCAR	NCAR	G, M, N	^d	Inside
PTR-ToF-MS	NCAR	NCAR	M	^e	Outside
CE-DOAS	CU	EUPHORE	G, M, N	^d	Outside Edge
BBCEAS	Leic	EUPHORE	G, M, N	^d	Center
PTR-ToF-MS	Leic	EUPHORE	M	^e	Outside Edge
Mad-LIP	UW	EUPHORE	G, M	^d	Outside Edge
W-DOAS	CEAM	EUPHORE	G, M, N	^d	Inside
EUPHORE FTIR	CEAM	EUPHORE	G, M	^d	Inside
SPME/GC-FID	CEAM	EUPHORE	G, M	^e	Outside Edge

^a Abbreviations given in the text.

^b Participants (CU – University of Colorado Boulder, USA; NCAR – National Center for Atmospheric Research, Boulder, CO, USA; Leic – University of Leicester, UK; CEAM – CEAM, Spain).

^c G – glyoxal (GLY), M – methyl glyoxal (MGLY), N – NO₂.

^d Concentration (molecule cm⁻³).

^e Volume mixing ratio referenced to temperature and pressure of the chamber as measured in the chamber.

Instrument inter-comparison of glyoxal, methyl glyoxal and NO₂

R. Thalman et al.

Title Page

Abstract

Introduction

Conclusions

References

Tables

Figures

◀

▶

◀

▶

Back

Close

Full Screen / Esc

Printer-friendly Version

Interactive Discussion



Table 2. Overview and description of experiments at NCAR(N) and EUPHORE(E).

Exp #	Date	Experiment Name	Description
N1	14 Jan 2011	Hydroxyacetone (HACET) + Cl	Methyl glyoxal comparison at 295 K
N2	14 Jan 2011	C ₂ H ₂ + Cl	Glyoxal comparison at 295 K
N3	14 Jan 2011	C ₂ H ₂ + OH	Glyoxal comparison at 295 K
N4	2 Feb 2011	HACET + Cl	Methyl glyoxal comparison at 295 K
N5	4 Feb 2011	HACET + Cl	Methyl glyoxal comparison at 295 K
N6	9 Mar 2012	C ₂ H ₂ + Cl	Glyoxal comparison at 295 K
N7	9 Mar 2012	HACET + Cl	Methyl glyoxal comparison at 295 K
N8	22 Mar 2012	HACET + Cl	Methyl glyoxal comparison at 320 K
N9	22 Mar 2012	C ₂ H ₂ + Cl	Glyoxal comparison at 320 K
E1 ^a	24 Jun 11	Glyoxal Inter-comparison	Injection of 40 ppbv of glyoxal followed by dilution to 10's of pptv
E2 ^a	27 Jun 2011	Methyl Glyoxal Inter-comparison	Injection of 20 ppbv of methyl glyoxal followed by sequential dilution to 100 pptv
E3 ^b	28 Jun 2011	<i>o</i> -xylene oxidation	photo-oxidation of <i>o</i> -xylene
E4 ^b	29 Jun 2011	Isoprene, High NO _x	In-situ generation of products of isoprene oxidation under high-NO _x conditions. OH production by photolysis of injected HONO.
E5 ^b	30 Jun 2011	O ₃ (A); O ₃ + C ₂ H ₂ (B)	(A) Chamber (Teflon) plus ozone and line residence times; (B) In-situ generation of glyoxal from the reaction of OH + acetylene (OH from TME + O ₃) in the presence of ozone in the dark
E6 ^b	1 Jul 2011	Ambient Air	Ambient Air filling the chamber followed by addition of NO _x and Isoprene (80 μL)
E7 ^b	4 Jul 2011	Isoprene, NO _x Control	Repeat of E4 with NO _x control working and lower initial isoprene to keep at lower NO _x levels in the chamber
E8 ^a	5 Jul 2011	Glyoxal Inter-comparison	Repeat of Exp 1
E8 ^b	5–6 Jul 2011	Glyoxal overnight dilution	Injection of 55 ppbv glyoxal and dilution overnight
E9 ^a	6 Jul 2011	NO ₂ interference with glyoxal	Addition of 10–200 ppbv of NO ₂ on top of ~300 pptv glyoxal
E10 ^a	6 Jul 2011	NO ₂ interference with Methyl Glyoxal	Repeat of E9 with the addition of 10–200 ppbv of NO ₂ on top of ~5 ppbv methyl glyoxal

^a Experiments with injection of glyoxal or methyl glyoxal.

^b Experiments with in-situ production of glyoxal/methyl glyoxal.

Instrument inter-comparison of glyoxal, methyl glyoxal and NO₂

R. Thalman et al.

Title Page

Abstract

Introduction

Conclusions

References

Tables

Figures

◀

▶

◀

▶

Back

Close

Full Screen / Esc

Printer-friendly Version

Interactive Discussion

**Table 3.** Correlation data for instruments vs. CE-DOAS for individual experiments.

Exp #	Species	Instrument	# pts	Slope	Intercept (ppbv)	R ²	Avg t (min)
Pure compound experiments							
NCAR ^a	GLY	FT-IR	19	1.02(2)	5(4) × 10 ^{11b}	0.996	4
NCAR ^a	MGLY	FT-IR	25	1.00(1)	1.2(7) × 10 ^{12b}	0.996	4
N7	MGLY	PTR-ToF-MS	5	0.95(3)	8.5(10) × 10 ^{12b}	0.997	4
NCAR ^a	NO ₂	FT-IR	80	1.06(2)	-2(4) × 10 ^{12b}	0.98	4
E1	GLY	BBCEAS	492	0.970(2)	-0.005(2)	0.9997	1
E1	GLY	Mad-LIP	338	0.82(1)	-0.003(1)	0.9998	1
E1	GLY	W-DOAS	284	0.917(3)	-0.06(1)	0.9998	1.5
E1	GLY	FT-IR	13	0.98(3)	0.1(7)	0.999	10
E1	GLY	SPME	15	0.95(10)	-0.01(1)	0.996	5
E1	GLY	CE-DOAS ^b	492	0.98(1)	0.17(10)	0.998	1
E8a	GLY	BBCEAS	546	0.967(5)	-0.012(2)	0.9998	1
E8a	GLY	Mad-LIP	528	1.11(2)	-0.002(3)	0.998	1
E8a	GLY	W-DOAS	239	0.916(7)	-0.07(2)	0.998	1.5
E8a	GLY	FT-IR ^c	53 ^c	0.99(2) ^c	-0.2(1) ^c	0.992	10
E8a	GLY	SPME	14	0.85(8)	0.00(1)	0.998	10
E8a low ^d	GLY	BBCEAS	316	1.009(9)	-0.021(3)	0.9994	1
E8a low ^d	GLY	Mad-LIP	239	1.17(2)	-0.006(4)	0.997	1
E8a low ^d	GLY	W-DOAS	144	0.68(5)	-0.03(2)	0.87	1.5
E2	MGLY	BBCEAS	503	1.010(3)	0.36(2)	0.9987	1
E2	MGLY	Mad-LIP	503	1.43(2)	-0.08(3)	0.997	1
E2	MGLY	FT-IR	55 ^c	1.174(13) ^c	0.65(13) ^c	0.996	10
E2	MGLY	PTR-ToF-MS	375	1.231(5)	-1.05(2)	0.96	10
E2	MGLY	W-DOAS	228	0.97(3)	-0.2	0.96	1.5

Table 3. Continued.

Exp #	Species	Instrument	# pts	Slope	Intercept (ppbv)	R^2	Avg t (min)
Mixed compound experiments							
E3	GLY	BBCEAS	348	0.988(3)	-0.012(2)	0.999	1
E3	GLY	Mad-LIP	211	0.83(1)	-0.034(2)	0.998	1
E3	GLY	W-DOAS	240	0.88(2)	-0.22(8)	0.97	1.5
E3	GLY	FT-IR ^c	58 ^c	1.5(1) ^c	0.95(10) ^c	0.88 ^c	10
E3	GLY	SPME	10	1.1(2)	0.08(2)	0.98	5
E3	MGLY	BBCEAS	316	0.92(2)	0.17(2)	0.97	1
E3	MGLY	Mad-LIP	240	1.66(3)	0.13(4)	0.95	1
E3	MGLY	FT-IR	58	1.3(1)	0.3(1)	0.99	10
E3	MGLY	SPME	10	0.86(13)	0.5(1)	0.65	5
E3	NO ₂	BBCEAS	345	1.0087(8)	0.046(3)	0.998	1
E3	NO ₂	W-DOAS	240	0.95(1)	0.14(2)	0.994	1.5
E5	GLY	BBCEAS	567	1.023(4)	-0.053(2)	0.99995	1
E5	GLY	Mad-LIP	241	^f	^f	^f	1
E5	GLY	FT-IR	79	1.07(1)	-0.4(1)	0.998	10
E6	NO ₂	BBCEAS	505	0.98(2)	0.02(2)	0.995	1
E6	GLY	BBCEAS	505	0.95(1)	-0.19(4)	0.987	1
E6	GLY	Mad-LIP	308	1.09(2)	-0.005(5)	0.97	1.5
E6	GLY	SPME	14	1.5(2)	0.04(5)	0.79	5
E6	MGLY	BBCEAS	505	0.68(3)	0.17(5)	0.68	1
E6	MGLY	Mad-LIP	308	1.90(6)	-0.1(1)	0.58	1.5
E6	MGLY	SPME	14	0.7(2)	0.2(2)	0.69	5
E7	NO ₂	BBCEAS	553	0.985(4)	-0.27(1)	0.999	1
E7	GLY	BBCEAS	553	0.927(3)	-0.034(3)	0.999	1
E7	GLY	Mad-LIP	326	1.47(2)	-0.033(6)	0.993	1.5
E7	GLY	FT-IR ^c	111 ^c	2.5(1) ^c	-0.2(1) ^c	0.93 ^c	10
E7	GLY	SPME	10	1.3(1)	0.04(4)	0.95	5
E7	MGLY	BBCEAS	553	0.92(1)	-0.20(4)	0.987	1
E7	MGLY	Mad-LIP	326	2.21(4)	0.6(1)	0.98	1.5
E7	MGLY	FT-IR ^c	111 ^c	0.68(4) ^c	-0.6(2) ^c	0.84 ^c	10
E7	MGLY	SPME	14	0.7(1)	1.3(5)	0.65	5

Number in is the 1- σ uncertainty of the last digit of the number.

^a NCAR experiment data is pooled over experiments listed in Table 2 (for GLY and MGLY) or for all oxidation experiments in 2011 and 2012 (30 + experiments at 3 different chamber temperatures).

^b Intercepts in molecules cm⁻³ due to the constant volume of the chamber and the changing pressure and temperature over the course of more than 30 different experiments (as described in note a).

^c Experiment near detection limit.

^d Only concentrations below 2 ppbv fitted for instruments with applicable detection limits.

^e Results from fit of the weak glyoxal bands (see Sect. 2.1.3).

^f Result is non-linear, Fig. S1 in Supplement.

Instrument inter-comparison of glyoxal, methyl glyoxal and NO₂

R. Thalman et al.

Title Page

Abstract

Introduction

Conclusions

References

Tables

Figures

◀

▶

◀

▶

Back

Close

Full Screen / Esc

Printer-friendly Version

Interactive Discussion



Instrument inter-comparison of glyoxal, methyl glyoxal and NO₂

R. Thalman et al.

Title Page

Abstract

Introduction

Conclusions

References

Tables

Figures

◀

▶

◀

▶

Back

Close

Full Screen / Esc

Printer-friendly Version

Interactive Discussion



Table 4. Detection limits of all instruments at NCAR and EUPHORE.

Instrument ^b	Precision (ppbv)	MGLY LOD _{report} ^c /LOD _{exp} ^d	Accuracy (%) ^a		Time (min.)
	GLY LOD _{report} ^c /LOD _{exp} ^d		GLY	MGLY	
CE-DOAS	0.015/0.012	0.15/0.27	–	–	1
NCAR FT-IR	50/–	92/–	–	–	4
NCAR PTR-ToF-MS ^d	–	–/1.2	–	–	0.167
CE-DOAS	0.015/0.012	0.21/0.27	–	–	1
BBCEAS	0.75/0.045	1.0/0.6	7	10 ^e	1
PTR-ToF-MS	–	0.53/5.3	–	–	1
Mad-LIP	0.06/0.038	1.2/0.9	53	80 ^e	1
W-DOAS	0.4/0.3	6.0/–	4	–	1.5
EUPHORE FTIR	2.5/1.1	2.7/–	150	70	10
SPME with GC-FID detection	0.1/–	0.15/–	50	20	10

^a Accuracy evaluated as the 95 % C.I. of the fitted slopes.

^b Abbreviations given in the text.

^c Reported Detection Limits 3 σ .

^d LOD measured during Exp 8b from Histograms in Figs. 9 and 10 for EUPHORE experiments and as the LOD in the instruments for other background data for NCAR (LOD = 3 σ , ppbv, see Sect. 4.2).

^e Omits Exp. E6 due to the lack of variability in the MGLY concentration (see Fig. 8c).

Instrument inter-comparison of glyoxal, methyl glyoxal and NO₂

R. Thalman et al.

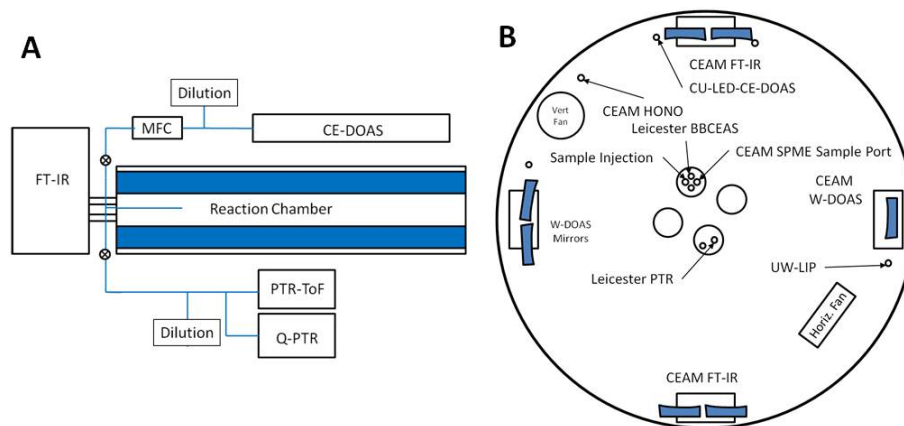


Figure 1. Layout of instruments at NCAR (a) and EUPHORE (b). In (b) small circles indicate sampling ports; the EUPHORE FTIR, W-DOAS and NCAR-FTIR light paths cross the entire chamber, while other instruments draw air from the chamber for analysis below/outside the chamber.

Instrument inter-comparison of glyoxal, methyl glyoxal and NO₂

R. Thalman et al.

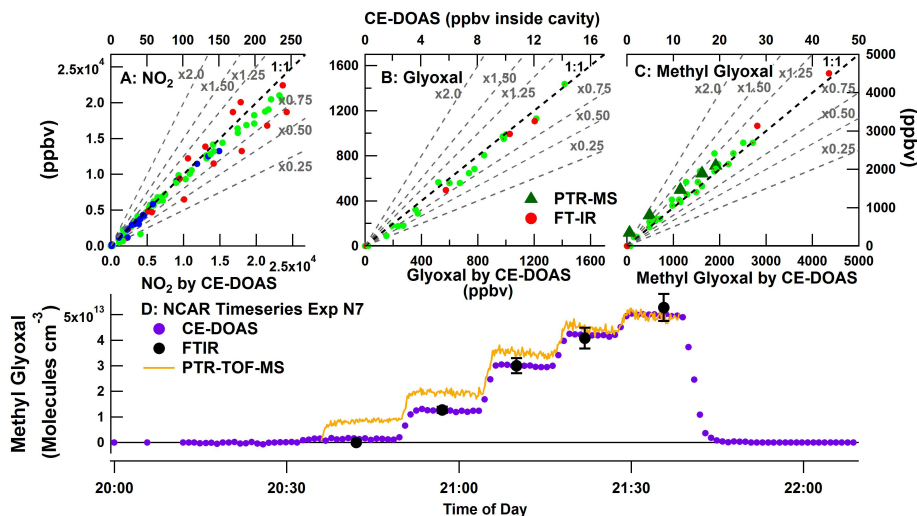


Figure 2. Correlation of FT-IR and PTR-ToF-MS relative to CE-DOAS for Experiments N1–N9 at NCAR (NO₂ includes additional experiments, see text). Data from individual experiments have been pooled at different temperatures. **(a–c)** FT-IR (dots), PTR-ToF-MS (triangles), three temperatures (blue – 260 K, green – 293 K, red – 330 K). **(d)** Shows a time series for experiment N7 to produce methyl glyoxal. Units of fit intercepts in **(a–c)** (molecules cm⁻³) have been converted to volume mixing ratios using the chamber temperature and pressure measured inside the chamber.

Title Page

Abstract

Introduction

Conclusions

References

Tables

Figures

◀

▶

◀

▶

Back

Close

Full Screen / Esc

Printer-friendly Version

Interactive Discussion



Instrument inter-comparison of glyoxal, methyl glyoxal and NO₂

R. Thalman et al.

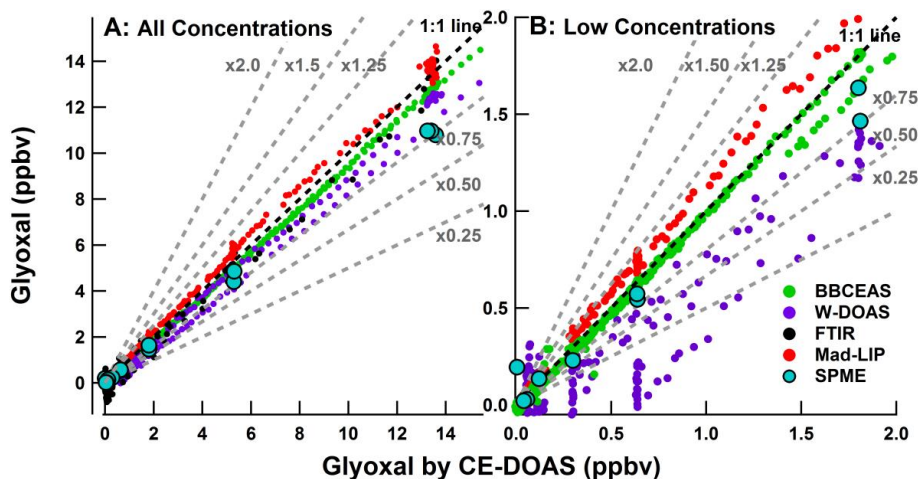


Figure 3. Correlations for the glyoxal comparison experiment E8a (see Fig. S2 in the Supplement for a time series of these points). **(a)** Shows the full concentration range; **(b)** shows concentrations below 2 ppbv. Data are only shown from instruments where the maximum concentration exceeds the LOQ (see Sect. 4.2).

Title Page

Abstract

Introduction

Conclusions

References

Tables

Figures



Back

Close

Full Screen / Esc

Printer-friendly Version

Interactive Discussion



Instrument inter-comparison of glyoxal, methyl glyoxal and NO₂

R. Thalman et al.

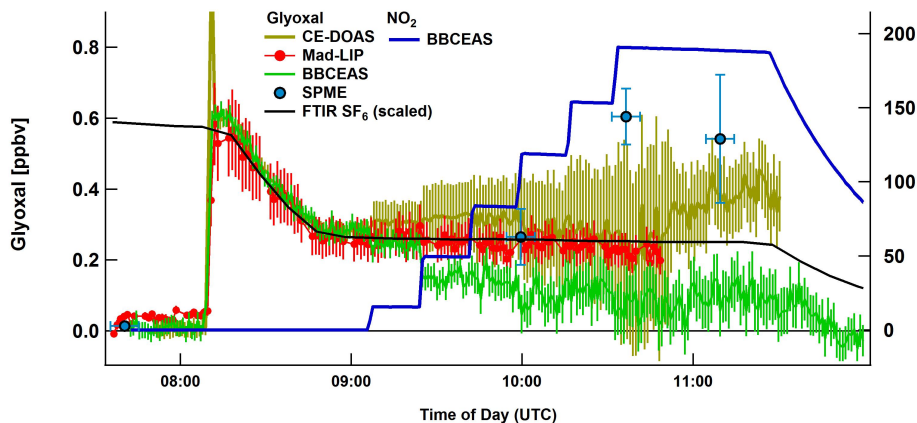


Figure 4. Sensitivity of glyoxal to high levels of NO₂ (Experiment E9). Chamber dilution has been scaled relative to concentrations at 0815 from the decay of the SF₆ tracer. See text for details.

[Title Page](#)[Abstract](#)[Introduction](#)[Conclusions](#)[References](#)[Tables](#)[Figures](#)[◀](#)[▶](#)[◀](#)[▶](#)[Back](#)[Close](#)[Full Screen / Esc](#)[Printer-friendly Version](#)[Interactive Discussion](#)

Instrument inter-comparison of glyoxal, methyl glyoxal and NO₂

R. Thalman et al.

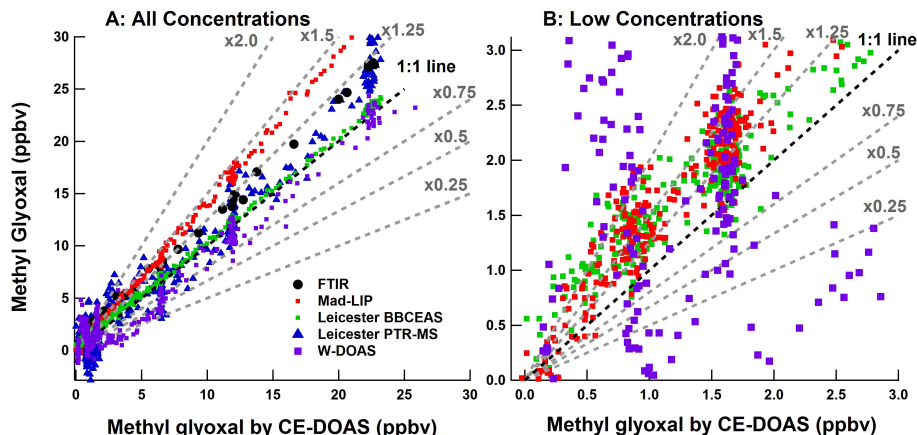


Figure 5. Correlation plots for methyl glyoxal comparison Experiment E2. **(a)** Shows the full range of measured concentrations, while **(b)** shows only concentrations below 3 ppbv. Only data is shown from instruments where the maximum concentration exceeds the LOQ (see Sect. 4.2).

[Title Page](#)[Abstract](#)[Introduction](#)[Conclusions](#)[References](#)[Tables](#)[Figures](#)[◀](#)[▶](#)[◀](#)[▶](#)[Back](#)[Close](#)[Full Screen / Esc](#)[Printer-friendly Version](#)[Interactive Discussion](#)

Instrument inter-comparison of glyoxal, methyl glyoxal and NO₂

R. Thalman et al.

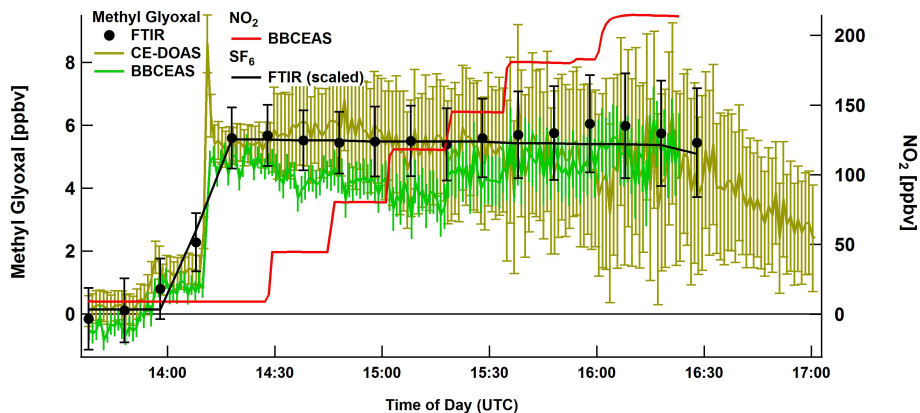


Figure 6. Sensitivity of methyl glyoxal to high levels of NO₂ from experiment E10. Chamber dilution has been scaled relative to concentrations at 14 : 10 from the decay of the SF₆ tracer. See text for details.

Title Page

Abstract

Introduction

Conclusions

References

Tables

Figures

◀

▶

◀

▶

Back

Close

Full Screen / Esc

Printer-friendly Version

Interactive Discussion



Instrument inter-comparison of glyoxal, methyl glyoxal and NO₂

R. Thalman et al.

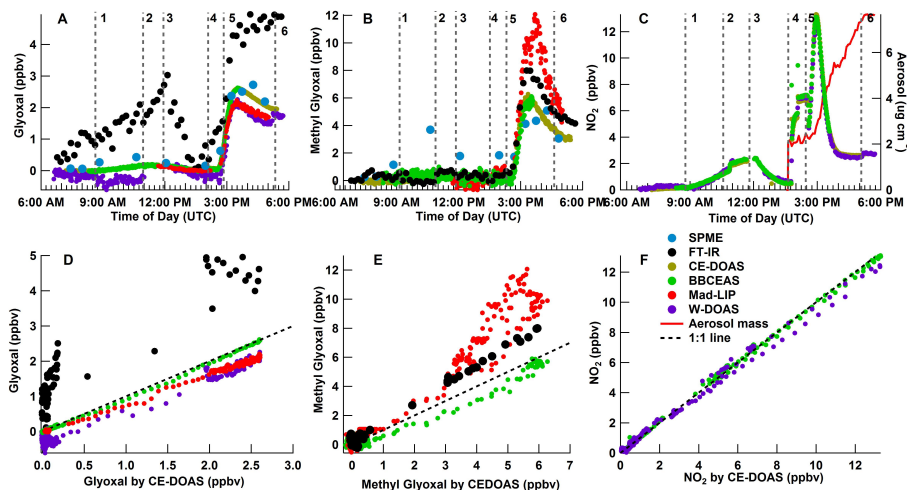


Figure 7. Dry photo-oxidation of *o*-xylene during Experiment E3. (a–c) Show the time traces of glyoxal, methyl glyoxal and NO₂, respectively. (d–f) Show the correlation plots of the respective compounds. E3 began in the morning with a clean, flushed chamber. The chamber roof was opened (1) while clean and the build-up of NO₂ and other contaminants was observed and then closed (2) and flushed clean (3). In the afternoon, HONO was added to the chamber (4) and with it some NO₂, then the chamber roof was opened (5) to initiate the photo-chemistry and closed to finish the experiment (6).

Instrument
inter-comparison of
glyoxal, methyl
glyoxal and NO₂

R. Thalman et al.

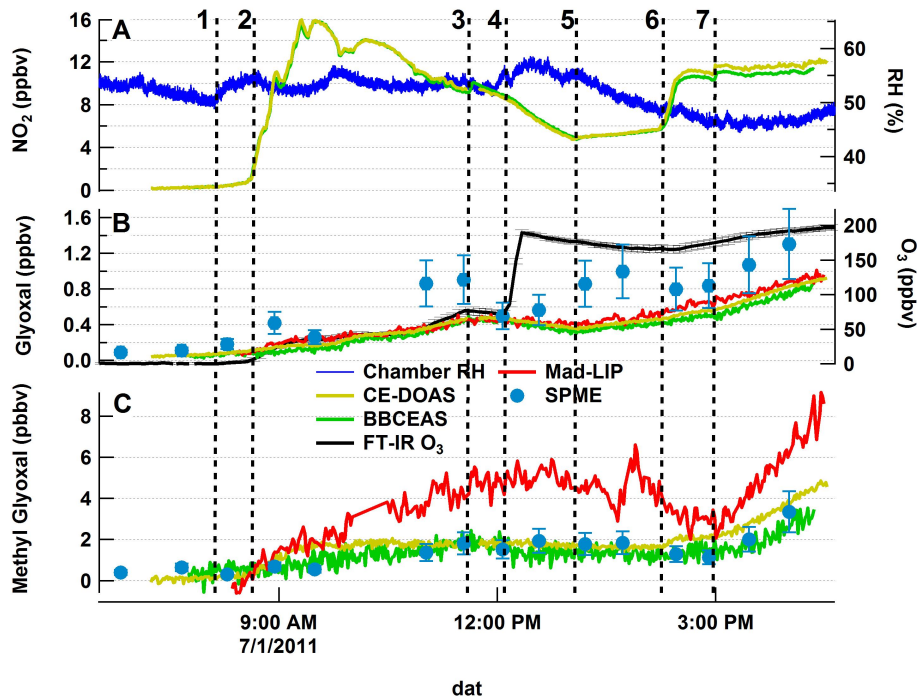


Figure 8. Ambient air experiment E6. **(a)** shows the NO₂ and relative humidity, **(b)** glyoxal and ozone, and **(c)** methyl glyoxal. The chamber operations for the day were as follows: (1) chamber roof open, (2) ambient air introduction, (3) chamber roof closed, (4) O₃ injection, (5) chamber roof open, (6) NO_x control on (HONO injection), (7) isoprene injection.

Instrument
inter-comparison of
glyoxal, methyl
glyoxal and NO₂

R. Thalman et al.

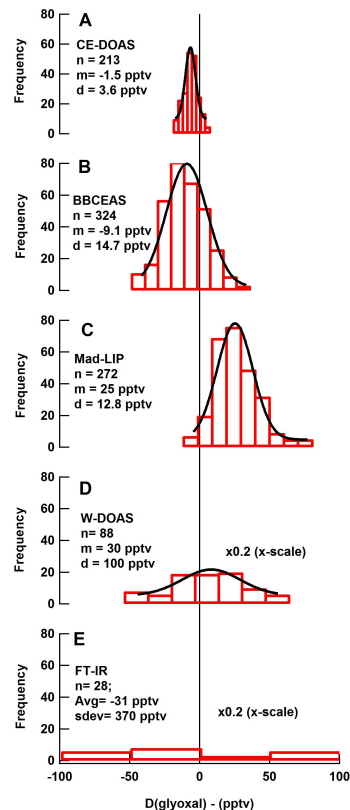


Figure 9. Histograms of glyoxal baseline variability during experiment E8b, 5 July 2011 from 02:00–06:00 UTC. The instruments sampled from a clean chamber. The number of points in the distribution (n), the mean (m) and $1\text{-}\sigma$ standard deviation (d) are listed on each graph, and experimentally determined limits of detection as quoted in Table 4 were calculated as $\text{LOD}_{\text{exp}} = 3 \cdot d$. The time series of the data used to produce the histograms is shown in Fig. S2 in the Supplement.

Instrument
inter-comparison of
glyoxal, methyl
glyoxal and NO₂

R. Thalman et al.

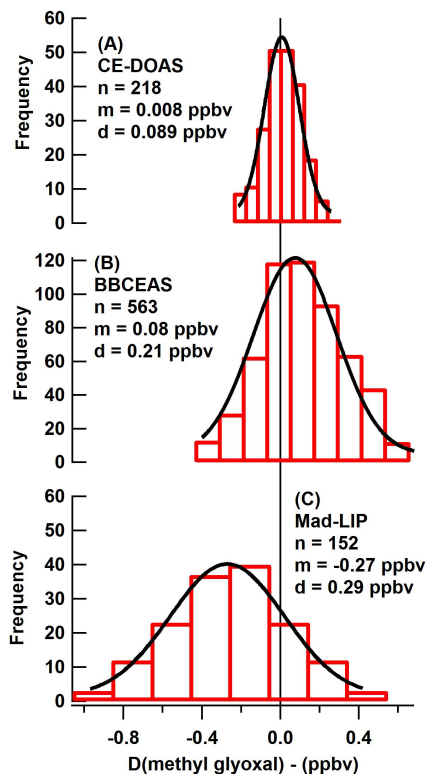


Figure 10. Histograms of methyl glyoxal baseline variability in experiment E8b. The number of points in the distribution (n), the mean (m) in ppbv and 1 standard deviation (d) of the distribution are listed in each panel (**a**: CE-DOAS; **b**: BBCEAS; **c**: Mad-LIP). Histogram distributions are used to calculate experimentally determined limits of detection as $\text{LOD}_{\text{exp}} = 3 \cdot d$.

[Title Page](#)[Abstract](#)[Introduction](#)[Conclusions](#)[References](#)[Tables](#)[Figures](#)[◀](#)[▶](#)[◀](#)[▶](#)[Back](#)[Close](#)[Full Screen / Esc](#)[Printer-friendly Version](#)[Interactive Discussion](#)